NAUB JOURNAL OF SCIENCE AND TECHNOLOGY
(NAUBJOST)
e-ISSN:2811-2350

Email: jost@naub.edu.ng http://journal.naub.edu.ng/naubjournal/

THERMAL AND STRUCTURAL STUDY OF SINTERED ANTIMONY OXIDE DOPED REDUCED GRAPHENE OXIDE (Sb_2O_3:RGO) COMPOSITE GLASS FORMER IN GLASS PRODUCTION APPLICATION

[1]M. Alpha., [1]A. Z. Ngari., [1]M. Jafaar., [2]Abore, M.D., [3]Y. B. Ahmed.
[1]Department of Physics, Nigerian Army University Biu, P.M.B 1500.Borno State
[2]Department of Chemistry, Nigerian Army University Biu, Borno State
[3]Department of Surveying, Nigerian Army University Biu, P.M.B 1500.Borno State

Corresponding Author: alpha.matthew@naub.edu.ng

Abstracts

This research was centered on investigating the structural and thermal phase transformations of an antimony trioxide reduced graphene oxide (Sb_2O_3:RGO) composite that can be used as glass former. Differential Thermal Analysis measurements (DTA) and structural analysis; a multi-technique approach (XRD and SEM) were used in this study. As the sintered temperature reduced from 800 ^{0}C to 750 ^{0}C, the average size of the crystallites for the composite increases. This encourages the creation of grown atomic layers, which provides a thermal energy gain mechanism that improves atomic restructuring and reduces crystal defects in sintered composites, as evidenced by dislocation density and micro strain values. Sintered Sb_2O_3:RGO at 750 ^{0}C had the highest transition temperature (711.4 ^{o}C), which matches the SEM result of the composite with the largest grain size.

Key Words: Glass former, Reduced Graphene Oxide, Sintering, Phase Transformation

Introduction

Antimony oxides (Sb_2O_3) were predicted to be glass former (Zachariasen, 1932; Shelby, 1997), and attempts to make vitreous antimony trioxide glass former have been made (Bednarik and Neely, 1982). However, all of the 'pure' glass components that have been developed so far seem to be the result of an unpremeditated constituent (principally SiO_2). Many preservatives, such as chlorine and water (Borgen and Krogh-Moe, 1956), have also been mentioned in vitreous antimony trioxide preparations, although they have not been thoroughly investigated.

Multiple heavy metal oxide glasses seem to have an extended infrared transmission region as well as non-linear optical properties, so the thermal properties of this impure Sb2O3 glass former may prove both fascinating and beneficial in glass production (Hasegawa *et al*., 1978; Zhao *et al*., 2013).

Nevertheless, the lack of clarity about the behavior of crystalline Sb_2O_3 prevents further study into these glasses. The goal of this work is to look into the thermal phase transformations of an antimony trioxide reduced graphene oxide composite used as glass former. For this research, a multi-technique approach was used, which included Differential Thermal Analysis (DTA) and structural studies (XRD and SEM).

Sand-silica (SiO_2) was most likely the first material used in glass making, but given the fact that many modern glasses comprise silica, it is not a core part of a glass. In reality, vitrification can be applied to a wide range of chemical substances; materials are classified as glasses based on their properties rather than their composition. A solid is classified as a glass if it meets two criteria: it has no deep order in its atomic arrangement and it has a 'glass transformation zone' (a time-dependent behaviour over temperature) (Lim *et al*., 2018; Meille *et al*., 2019). Over a broad temperature range, the glass transformation area occurs. However, identifying a single glass transition temperature, T, as an indicator of the onset of the glass transformation area when the glass is heated is often useful (Masuda *et al*., 1995).

Even though some glass formers, such as B_2O_3, may form vitreous systems on their own, other, less capable glass formers, such as Sb_2O_3, require more severe cooling rates (Wang *et al*., 2020).The creation of a continuous random network of atoms, as opposed to the ordered, repeated atomic structure in a crystal lattice, is required by glass structural theories. This can be facilitated in weak glass formers by introducing a small amount of contaminant which in this case, the reduced graphene oxide.

Experimental

10 g of commercial Sb_2O_3 was dry milled in a Retsch PM 400 planetary ball mill using stainless steel balls and vials (250 ml capacity) at 300 rpm, with a 1:20 powder to ball weight ratio. Milling was undertaken for 6 hours. The obtained slurries were dried at 120 ^{0}C for 4 hours and then sieved with a 30-mesh sieve (particle size ~550 μm). The reduced graphene oxide was synthesis using an improved modified hummer method as described by Alpha *et al.* 2019. For preparation of the composite glass former, the fine powders samples of Sb_2O_3 and reduced graphene oxide were placed in graphite crucible directly, heated up with the heating rate of 5 ^{0}C/min, to a sintering temperature of 750 ^{0}C and 800 ^{0}C, and kept at temperature for 30 minutes. The obtained glass former composite samples (Sb_2O_3:RGO) were naturally cooled down to room temperature and cut into samples for measurements.

XRD Results

Sb_2O_3 was classified as pure senarmontite by an XRD scan, as shown in figure 1. 1. From this, it was clear that senarmontite peaks could be found in commercial material. The average crystallite size (D) of the pure senamontite was calculated using Debye Scherer's formula:

$$D = \frac{0.9\lambda}{\beta cos\theta} \quad (1)$$

where β = full width at half maximum (FWHM), θ = diffraction angle, k = Shape factor and λ = wavelength of the X-rays (1.5406 Å).

Dislocation density δ was calculated using (Daniel *et al*., 2019).

$$\delta = \frac{1}{D^2} \quad (2)$$

The micro-strain ε was estimated using the equation (Daniel *et al*., 2019).

$$\varepsilon = \frac{\beta}{4tan\theta} \quad (3)$$

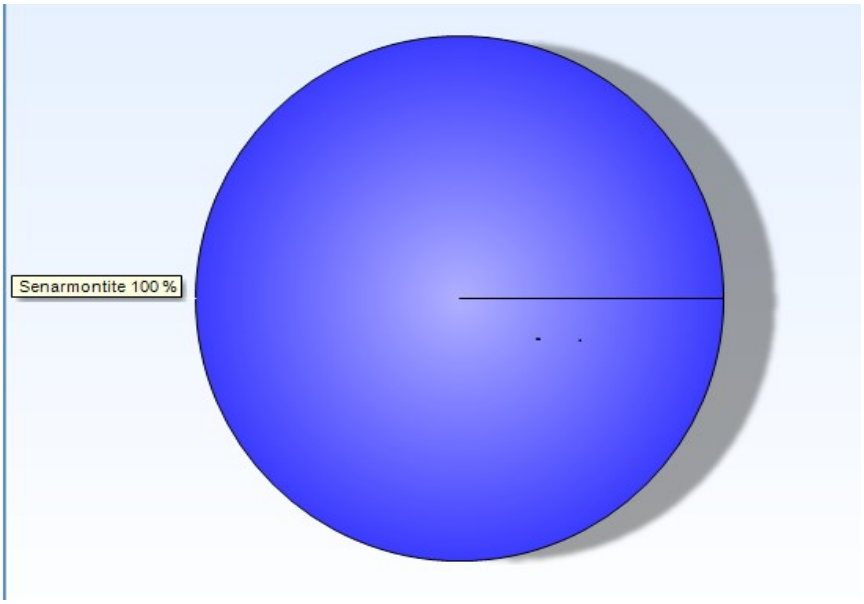

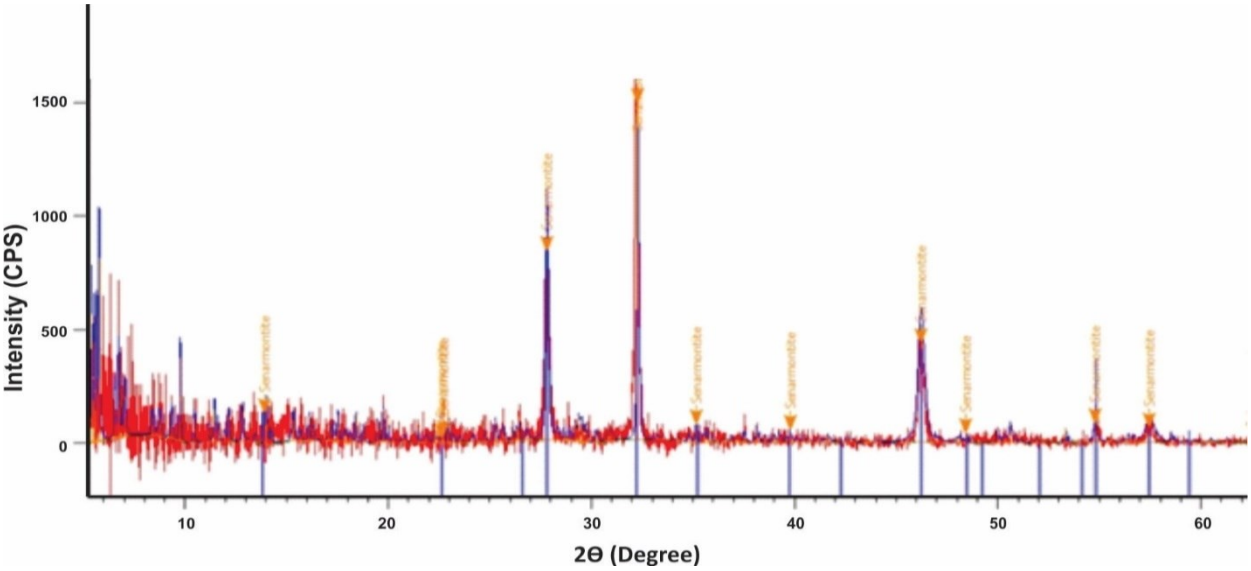

Figure 1.1 pure senarmontite

Figure 1.2 XRD spectra of Sb_2O_3

After sintering, the x-ray diffraction patterns (Fig. 1.3b) of the composite samples transitioned to valentinite. The peaks that were obtained were considerably wider than those obtained with the other crystalline samples. These may be caused by strain or crystallite size, which has an agglomeration tendency. Lowering the sintering temperature is necessary not only to improve thermal efficiency, but also to prevent the glass former from crystallising, since extreme crystallisation will hinder the stability of the already formed composite.

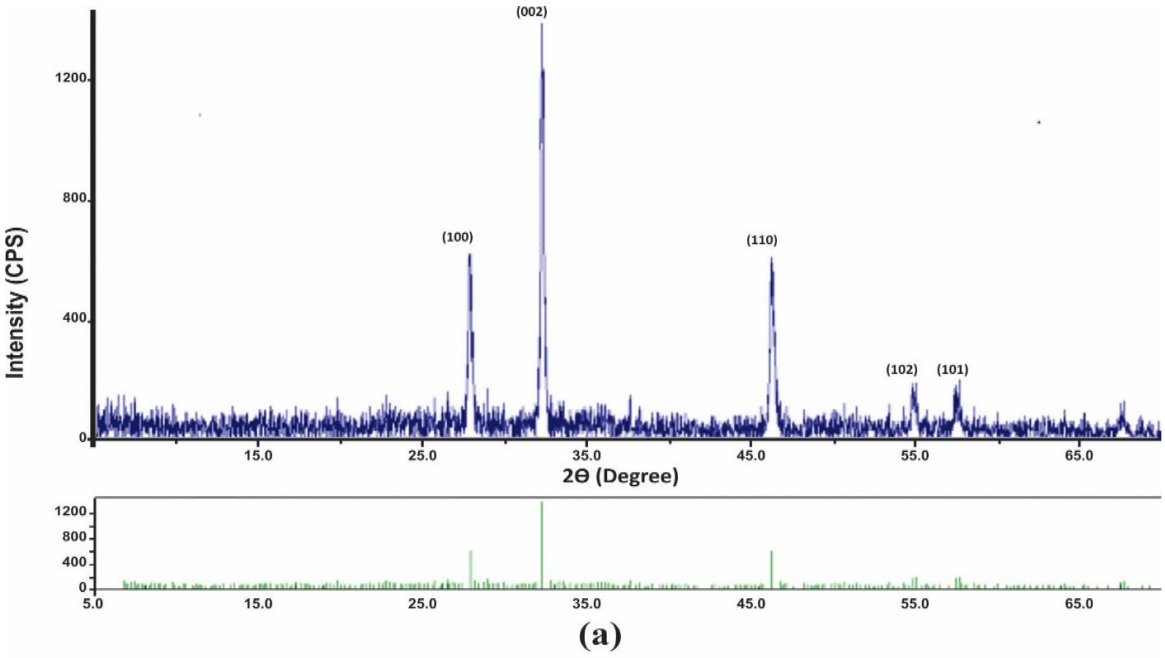

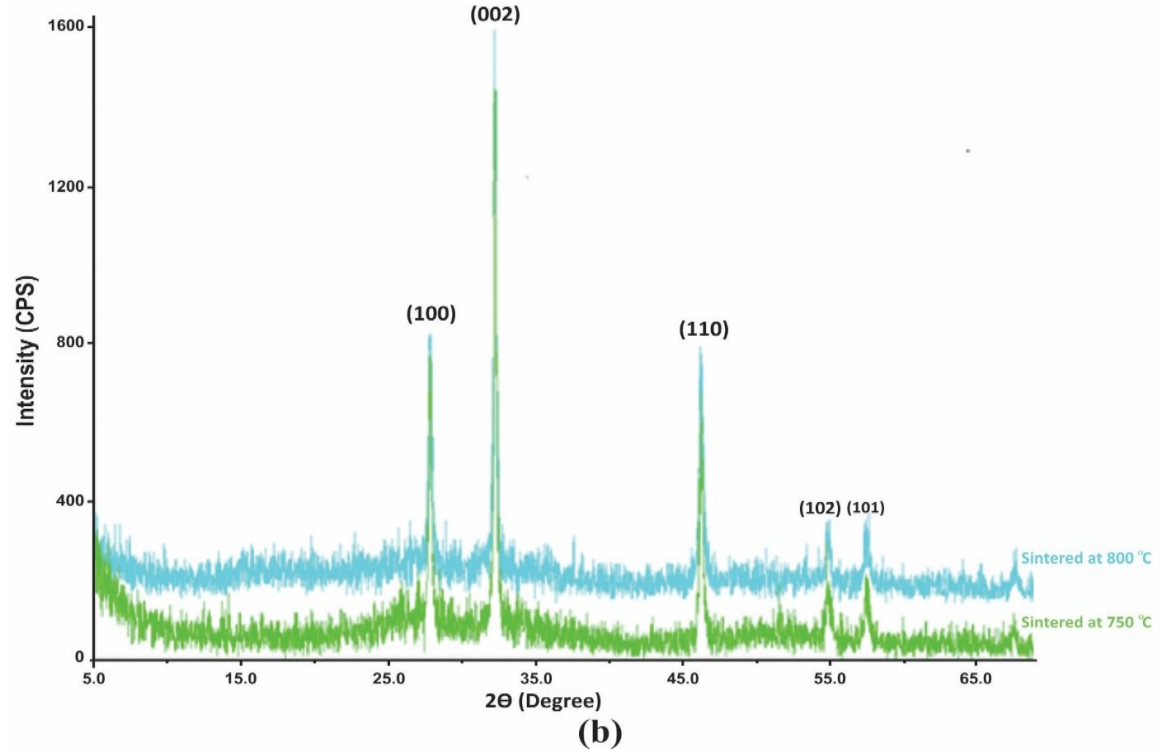

Figure 1.3 XRD spectra of composite (a) Unsintered Sb_2O_3:RGO and (b) Sintered Sb_2O_3:RGO

Table 1: Summary of calculated structural parameters for the composites

S/n	Sample	2Θ (°)	Full width Half maximum $\boldsymbol{\beta}$ (°)	Crystal Size D (nm)	Dislocation density $\boldsymbol{\delta \times 10^{14}}$ (Lines/$\boldsymbol{m^2}$)	Micro strain $\boldsymbol{\varepsilon \times 10^{-4}}$
1	Unsintered Sb_2O_3:RGO	31.75091	0.12333	66.94	2.23	4.69
2	Unsintered Sb_2O_3:RGO at 800 ^{0}C	31.73912	0.13633	60.57	2.73	5.72
3	Sintered Sb_2O_3:RGO at 750 ^{0}C	31.70270	0.15030	67.94	3.31	6.30

The full width at half the maximum of the most desired orientation (002) was used to calculate the average crystallite size of the sample. The average size of the crystallites was found to increase as the sintered temperature was decreased from 800 ^{0}C to 750 ^{0}C. This facilitates the formation of grown atomic layers that creates a thermal energy gain system which enhances atomic restructuring leading to a decrease in crystal defects in the sintered samples as revealed by the values dislocation density and the micro strain in table 1.

SEM Results

The composites' SEM morphology and cross section show a uniform and homogeneous structure with few distinct microstructures consisting of a section of agglomerates and some established spherical grains (fig 1.4a&b). Decreasing the sintering temperature (to 750 ^{0}C) culminated in a more uniform structure with tightly bound grains, which improved grain and crystal structure by revealing the deeper layers of the atoms to stronger interatomic forces, resulting in the formation of a given compact structure (fig. 1.4c).

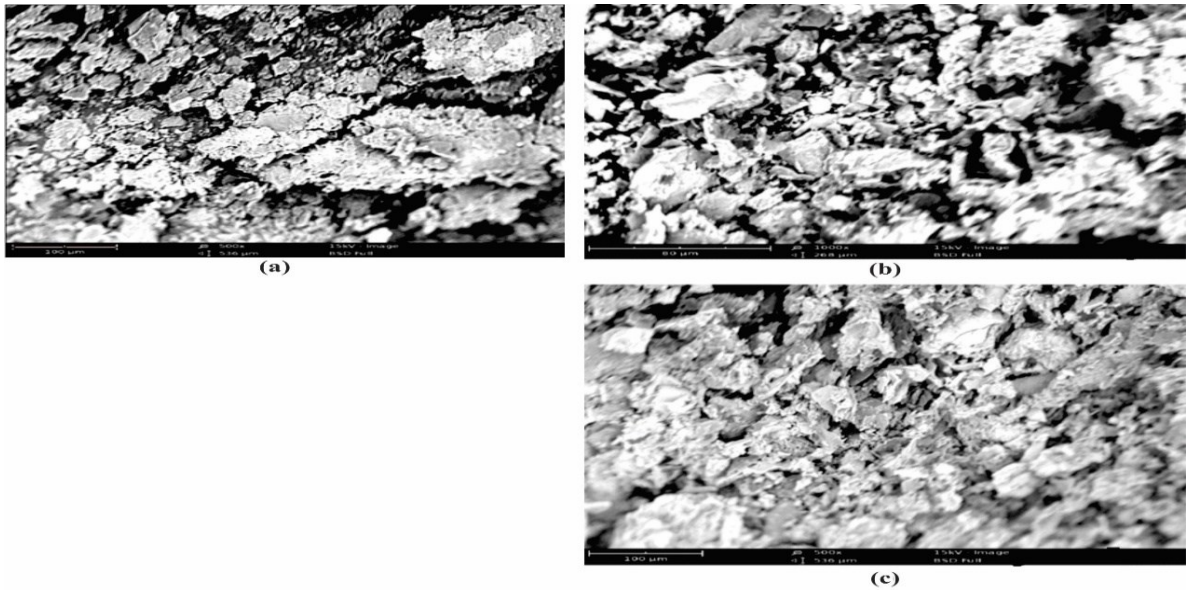

Figure 1.4 SEM images of (a) Unsintered Sb_2O_3:RGO (b) Unsintered Sb_2O_3:RGO at 800 ^{0}C and (c) Sintered Sb_2O_3:RGO at 750 ^{0}C

Figure 1.5 Grain size histogram of (a) Unsintered Sb_2O_3:RGO (b) Unsintered Sb_2O_3:RGO at 800 ^{0}C and (c) Sintered Sb_2O_3:RGO at 750 ^{0}C

The average grain size from the SEM image of the samples was determined using imageJ software, as shown in figure 1.5. A non-uniform grain concentration is visible in the histogram. At grain sizes ranging from 0.0 to 1400 µm, there is a broad distribution. The grain size distribution for unsintered Sb_2O_3:RGO is greater at 800 to 1000 µm than at other ranges (fig 1.5a). At 200 to 400 µm for the sintered composite (fig 1.5b&c), a preferred grain distribution and growth defining factor or pattern occurs, which could be related to the preferred orientation, and could also be due to initialisation of grain stability and uniformity at that range.

DTA Result

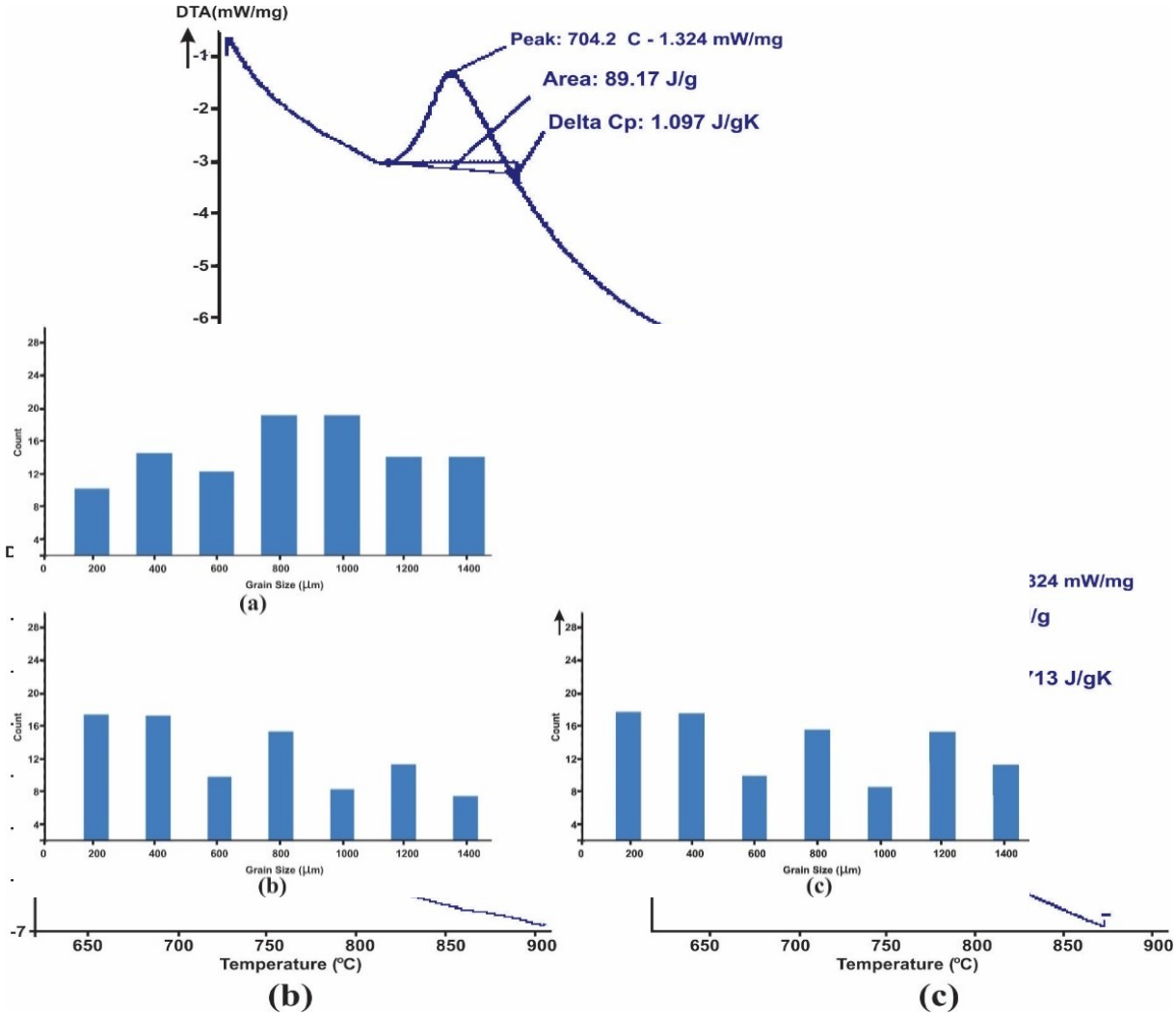

In addition, the peaks of the samples at the transition temperature are wider (Fig 1.6). This means that the phase transition does not happen all at once, but rather happens progressively over a temperature range.

Figure 1.6 DTA Spectra of (a) Unsintered Sb_2O_3RGO (b) Unsintered Sb_2O_3:RGO at 800 ^{0}C and (c) Sintered Sb_2O_3:RGO at 750 ^{0}C

This is attributable to Sb atoms occupying off-centred positions, in which order-disorder characteristics between off-centred Sb ions could be direct or phonon-mediated, and displaced characteristics relating to translational changes of RGO and O sub-lattices having a significant impact on the phase transition. This triggers a dielectric anomaly, which gets worse as the phase transition gets longer. The XRD results revealed these defects and changes in the crystalline structure (figure 1.3). The sample with the highest transition temperature (711.4 ^{0}C) was (Sb_2O_3: RGO at 750 ^{0}C), which matches the SEM result of the sample with the maximum grain size.

Conclusion

In conclusion the average size of the crystallites was found to increase as the sintered temperature was decreased from 800 ^{0}C to 750 ^{0}C. This facilitates the formation of grown atomic layers that creates a thermal energy gain system which enhances atomic restructuring leading to a decrease in crystal defects in the sintered samples as revealed by the values dislocation density and the micro strain. The sample with the highest transition temperature (711.4 ^{0}C) was (Sb_2O_3:RGO at 750 ^{0}C), which matches the SEM result of the composite with the maximum grain size.

References

Alpha, M., Uno, U.E., Isah, K.U., & Ahmadu, U. (2019). Structural and Electrochemical Properties of Reduced Graphene Oxide (RGO) Synthesised Using an Improved Modified Hummers Method as Electrode Material for Electronics Applications. *Nigerian Journal of Technology (NIJOTECH)*, 38(4), 997 – 1002

Bednarik, J. F. & Neely, J. A. (1982). *Glastechn. Ber.* 55 (1982). A single component antimony oxide glass and some of its properties, *Glass Tech. Ber*., 55, 126–129

Borgen, O., & Krogh-Moe, J. (1956). On the structure of oxide glasses. *Acta Chem. Scand.* 10(2), 265-267.

Daniel, T.O., Uno, E.U., Isah, K.U., &Ahmadu.U. (2019). Electric double layer field effect Transistor using SnS thin film as semiconductor channel layer and honey gate dieletric. *East European Journal of Physics,* 3, 71-80. https://doi.org/10.26565/2312-4334-2019-3-09

Hasegawa, H., Sone, M., & Imaoka, M. (1978). X-ray Diffraction Analysis on the Structure of the Glasses in the System PbO-SiO2. *Journal of Non-Crystalline Solids*, 85, 393-412*,* 19(2), 28-33.

Lim, K. Y., Kim, Y. W., & Song, I. H. (2018). Low-temperature processing of porous SiC ceramics," *Journal of Materials Science* 48(5), 1973–1979.

Masuda, H., Ohta, Y., & Morinaga, K. (1995). Crystallite properties of glass. *J. Japan Inst. Metals,* 59(1), 31-36.

Meille, S., Lombardi, M., Chevalier, J., & Montanaro, L. (2019). Mechanical properties of porous ceramics in compression: on the transition between elastic, brittle, and cellular behavior, *Journal of the European Ceramic Society*, 32(15), 3959– 3967.

Shelby, J. E. (1997). Introduction to Glass Science and Technology, *Royal Society of Chemistry*, 1997.

Wang, X., Chen, X., & Lu, A. (2020). Study of foam glass with high content of fly ash using calcium carbonate as foaming agent, *Materials Letters*, 79, 263–265.

Zachariasen, W. H. (1932). The Atomic Arrangement in Glass. *Journal of the American Chemical Society,* 54, 3841-3851.

Zhao, J., Zhu, Y., Li, Z., & Lv, X. (2013). Effect of Bi_2O_3 on physical properties of vitrified bond and mechanical properties of diamond composites," *Materials Science and Engineering*, 568, 102–107.